Talanta 225 (2021) 121957

Contents lists available at ScienceDirect

Talanta

journal homepage: www.elsevier.com/locate/talanta

Epoxy-functionalized macroporous carbon with embedded platinum nanoparticles for electrochemical detection of telomerase activity via telomerase-triggered catalytic hairpin assembly

Huixian Jia [a], Ningzhao Shang [b], Xiaobo He [a], Anaclet Nsabimana [c], Danna Sun [a], Huan Wang [a], Yufan Zhang [a,*]

[a] Key Laboratory of Medicinal Chemistry and Molecular Diagnosis of the Ministry of Education, Key Laboratory of Analytical Science and Technology of Hebei Province, College of Chemistry and Environmental Science, Institute of Life Science and Green Development, Hebei University, 071002, Baoding, PR China
[b] College of Science, Hebei Agricultural University, 071001, Baoding, PR China
[c] Chemistry Department, College of Science and Technology, University of Rwanda, Po Box: 3900, Kigali, Rwanda

ARTICLE INFO

Keywords:
Telomerase activity
Electrochemical biosensor
Catalytic hairpin assembly
Ultra-sensitivity detecting

ABSTRACT

Telomerase is regarded as a crucial biomarker for the early diagnosis of malignant tumors and a valuable therapeutic target. In this work, a telomerase-triggered amplification strategy was designed on the basis of a catalyzed hairpin assembly (CHA) for bridging a signal probe of platinum nanoparticles (Pt NPs) anchored on three-dimensional (3D) epoxy-functionalized macroporous carbon (Pt/MPC-COOH) in an ultrasensitive electrochemical biosensor. Pt/MPC-COOH nanomaterials with interconnected macroporous structure not only immobilized hairpin DNA probe 2 (H2) via an amide reaction (Pt/MPC-COOH-H2), but they also generated an obvious electrochemical signal in response to acetaminophen (AP) oxidation. After the introduction of telomerase, telomerase primer (TP) was extended to a telomerase extension product (TEP) with several hexamer repeats (TTAGGG)n to initiate the CHA cycle, leading to signal amplification. Subsequently, with the TEP-triggered CHA cycle amplification strategy, a large amount of Pt/MPC-COOH-H2 was introduced on the electrode surface for the construction of the electrochemical platform, which realized the sensitive detection of telomerase activity from 10^2 to10^7 cells mL^{-1} with a limit of detection (LOD) of 9.02 cells mL^{-1}. This strategy provides a sensitive method for the detection of biomolecules that could be useful for bioanalysis and early clinical diagnoses of diseases.

Credit author statement

Huixian Jia, Methodology; Software; Writing – original draft, Ningzhao Shang: Writing- Reviewing and Editing, Xiaobo He: Investigation; Methodology; Data curation, Anaclet Nsabimana: Data curation; Writing – original draft, Danna Sun: Investigation; Methodology; Data curation, Huan Wang: Writing- Reviewing and Editing, Funding acquisition, Yufan Zhang: Investigation; Methodology; Data curation; Software; Supervision; Funding acquisition.

1. Introduction

Telomerase is a ribonucleoprotein that preserves telomeric length and stability by catalyzing the addition of repeat units (TTAGGG)n onto the 3' ends of telomeres through its reverse transcriptase and endogenous RNA template [1–5]. It is well-known that in 85% of malignant tumor cells, telomerase is highly reactivated, and thus, telomerase can be considered as a remarkable biomarker for the identification and therapy of tumor cells [6,7]. Therefore, sensitive and accurate quantification of telomerase activity is of crucial importance for bioanalysis and early clinical diagnoses of disease [8–10]. One of the most powerful approaches for telomerase activity detection is the polymerase chain reaction (PCR)-based telomere repeat amplification protocol (TRAP). Although the sensitivity of this method is ultrahigh, it is limited by harsh reagent storage conditions, unstable enzymatic activity, and highly technical manipulation [7,11–14]. To overcome the above-mentioned shortcomings, several alternative PCR-free methods such as electrochemiluminescence [15], fluorescence [16], colorimetry [17], and electrochemical method [18–23] have been developed to determine telomerase activity. Among them, electrochemical methods

* Corresponding author.
E-mail address: zyf@hbu.edu.cn (Y. Zhang).

https://doi.org/10.1016/j.talanta.2020.121957
Received 27 September 2020; Received in revised form 21 November 2020; Accepted 1 December 2020
Available online 3 December 2020

have been widely utilized to detect telomerase activity because of their simple operation, high sensitivity, rapid response, and low cost. For example, Liu et al. described the electrochemical strategy for telomerase activity detection based on T7 exonuclease-aided target recycling amplification [18]. Ling P. et al. Described the electrochemical assay of telomerase activity by platinum nanoparticles encapsulated in metal-organic frameworks as a signal indicator [24].

There has been great interest in three-dimensional (3D) macroporous carbon (MPC) with continuously interconnected macroporous structures, and it has been used in many research areas such as sensors, biomimetic catalysis, and catalyst support [25–27]. MPC exhibits a unique macroporous structure, remarkable electrical conductivity, large pore volume and specific surface area, satisfactory chemical inertness, and thermal stability, and thus, it is a suitable platform for loading other species to fabricate novel composites with excellent synergetic effects [28–30]. In particular, epoxy-functionalized MPC can provide a strong support for binding with DNA by the biochemical self-assembly process due to the many –COOH sites on its surface.

One electrode material that has the potential for widespread use is the noble-metal/carbon composite. Noble-metal nanoparticles (NMNPs), a type of high-performance electrocatalyst, exhibit unique electrocatalytic characteristics [31,32]. Because of the synergistic effects between the uniformly dispersed NMNPs and the continuously interconnected macroporous structures of MPC, the NMNPs/MPC composites exhibit remarkable electrical conductivity and electrocatalytic properties [33–35]. Because of these characteristics, NMNPs/MPC composites can be used as a signal probe to detect telomerase activity.

Herein, we report a simple and sensitive strategy to detect telomerase activity in malignant tumors by combining Pt/MPC-COOH as a signal probe and the telomerase-triggered CHA process as a unique signal amplifier. The detailed mechanical principle is depicted in Scheme 1. Pt/MPC-COOH nanomaterial with an interconnected macroporous structure not only immobilized hairpin DNA probe 2 (H2) via an amide reaction (Pt/MPC-COOH-H2), but it also generated an obvious electrochemical signal towards acetaminophen (AP) oxidation. After the introduction of telomerase, the telomerase primer (TP) was extended to a telomerase extension product (TEP) with several hexamer repeats (TTAGGG)n. The TEP subsequently opened hairpin DNA probe 1 (H1) modified on electrode surfaces, and then, H2 on Pt/MPC-COOH-H2 replaced TEP. The released TEP then entered the next cycle to open the next H1. Importantly, a mass of Pt/MPC-COOH-H2 can be introduced on the electrode surface, resulting in an increased electrochemical signal of the readout. Therefore, the proposed electrochemical sensing platform can achieve sensitive detection of biomolecules in low concentrations, which enhances its diagnostic efficiency.

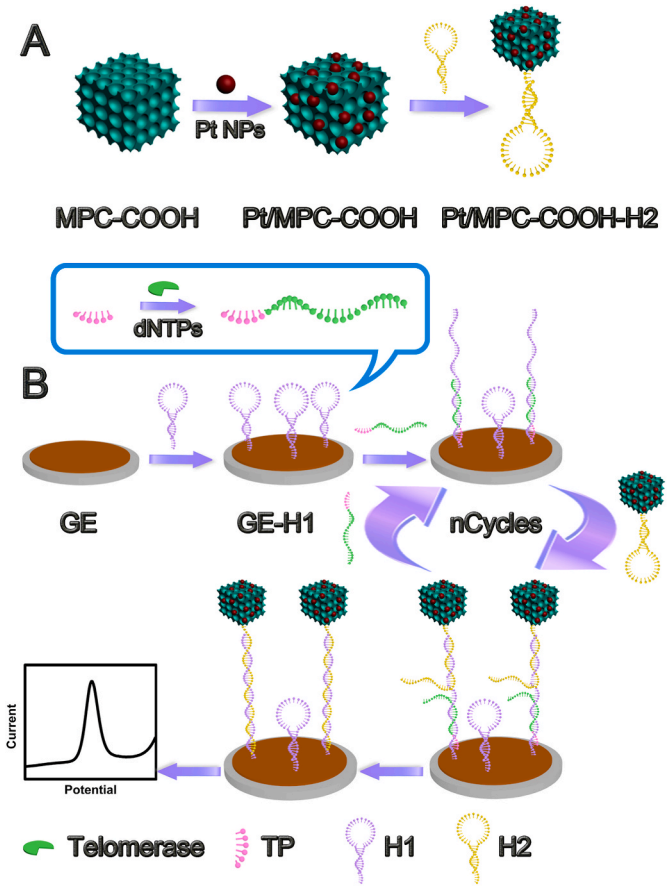

Scheme 1. Preparation of the Pt/MPC-COOH nanomaterial (A). Schematic representation of the fabrication process of the biosensor (B).

2. Experimental section

2.1. Reagents and materials

The 6-Mercapto-1-hexanol (MCH), N-Hydroxysuccinimide (NHS), 3′-Azido-3′-deoxythymidine (AZT), and 1-Ethyl-3-(3-(dimethylamino) propyl) carbodiimide hydrochloride (EDC) were supplied by Aladdin Inc. (Shanghai, China). Succinic anhydride, magnesium chloride ($MgCl_2$), 2-mercaptoethanol, Tween 20, ethylene glycol bis(2-aminoethylether)-N,N,N,N-tetraacetic acid (EGTA), phenylmethylsulfonyl fluorid (PMSF), bovine serum albumin (BSA), tris-(hydroxymethyl) aminomethane (tris), glycerol, isopropanol, 3-[(3-cholamidopropyl) dimethylammonio]-1-propanseulfonic acid (CHAPS), polyoxometalates (POMs), sucrose, tris(2-carboxyethyl)-phosphine (TCEP), and chloroplatinic acid ($H_2PtCl_6{\cdot}6H_2O$) were purchased from Macklin Biochemical Co. Ltd (Shanghai, China). All DNAs and the deoxynucleotide mixture (dNTPs) were purchased from Shanghai Sangon Biological Engineering Technology & Services Co. Ltd. (China), and the sequences are shown in Table S1. H1and H2 were heated to 90 °C for 5 min and then gradually cooled down to room temperature before use. The used buffers are DNA washing buffer (10 mM Tris-HCl, pH = 7.4), DNA reserve buffer and hybridization buffer:1 × TE buffer (10 mM Tris-HCl, 1.0 mM NaCl, pH = 7.4). All aqueous solutions were prepared with ultrapure water (>18 MΩ, Millipore).

2.2. Instruments

Electrochemical measurements were implemented with a PGSTAT 302N Autolab Electrochemistry Workstation (Metrohm, Switzerland). The classical three-electrode, consisting of a gold electrode (GE) or a modified electrode as working electrode, a platinum wire as auxiliary electrode, and an Ag/AgCl as reference electrode. Scanning electron microscopy (SEM; Philips XL-30) and transmission electron microscopy equipped with EDX (TEM; JSM- 6700F, Japan) were used to record the morphology of the products. The X-ray diffraction (XRD) for the crystal structure analysis of nanomaterials was examined on a X-ray D/max-2200vpc diffractometer with Cu Kα X-ray source. The zeta potentials of materials were obtained on a Zeta Potentials Analytical Instruments (Brookhaven Instruments, USA). The surface functional types of materials were investigated by Fourier transform infrared (FT-IR) spectroscopy (Nicolet Magna 560). X-ray photoelectron spectroscopy (XPS, thermo ESCA LAB spectrometer, USA) was applied for elemental analysis of synthesized nanomaterials.

2.3. Cell culture

HeLa, MCF-7, A549, and MDA-MB-231 cells were grown in Dulbecco's modified Eagle's medium (DMEM) supplemented with streptomycin (100 μg mL^{-1}), penicillin (100 μg mL^{-1}), and 10% fetal bovine serum (FBS) in a 37 °C incubator with 5% CO_2. For telomerase

extraction, 1.72×10^7 cells were transferred into an EP tube, washed twice with ice-cold phosphate-buffered saline (PBS, 0.1 M, pH 7.4), and redispersed in ice-cold CHAPS lysis buffer consisting of (Tris-HCl (10 mM pH 7.5), glycerol (10%), CHAPS (0.5%), 2-mercaptoethanol (5 mM), $MgCl_2$ (1 mM), PMSF (0.1 mM), and EGTA (1 mM). After that, the cells were redispersed in ice-cold CHAPS lysis buffer and incubated for 30 min on ice. After centrifugation for 20 min (12,000 rpm, 4 °C), the supernatant was carefully transferred to a new tube and used immediately or frozen at −80 °C. For the inhibition experiments, different volumes of AZT (20 mM) solutions were added to the telomerase extension reaction buffer to achieve the desired final concentrations. For the control experiment, telomerase extracts were heat-treated at 95 °C for 10 min.

2.4. Preparation of epoxy-functionalized MPC and Pt/MPC-COOH

MPC was performed according to the previous reports [36,37]. Prior to use, the 0.45 g MPC powder was dissolved in 1 M HNO_3 solution (75.00 mL) and refluxed at 90 °C for 6 h to obtain the epoxy-functionalized MPC. The epoxy-functionalized MPC samples were collected by centrifugation and dried in air (100 °C). For Pt/MPC-COOH, 30 μL of isopropanol was mixed in 1.5 mL of the POMs (10 mg mL^{-1}) solutions. The reaction mixture was irradiated for 30 min under ultra-violet light (500 W) until a blue solution was obtained. After that, 12 μL of $H_2PtCl_6{\cdot}6H_2O$ (100 mg mL^{-1}) and 200 μL of epoxy-functionalized MPC suspension 5 mg mL^{-1}) were injected into the above blue solution under stirring for 5 min. The resulting products were collected by suction filtration and washed with double distilled water. Finally, the products were obtained after drying at 80 °C overnight.

2.5. Construction of Pt/MPC-COOH-H2

The Pt/MPC-COOH-H2 was prepared through the covalent interaction between the –COOH groups of Pt/MPC-COOH and $–NH_2$ groups of H2. First, 200 μL of Pt/MPC-COOH (1.0 mg mL^{-1}) aqueous solution was added to 500 μL of EDC (20 mg mL^{-1}) and NHS (10 mg mL^{-1}) solution, and incubated for 2 h at room temperature. After that, 500 μL of DNA (10 μM) was added to the Pt/MPC-COOH suspension, slightly shaken for 12 h at 4 °C, and centrifuged for 20 min at 12,500 rpm to remove excess EDC and NHS. The conjugated Pt/MPC-COOH-H2 was finally dispersed in 0.1 M PBS buffer (pH 7.4) and stored at 4 °C for later use.

2.6. Fabrication of the proposed biosensor

The GE was carefully polished with 1, 0.3, and 0.05 μm alumina powder, and then, it was washed in ethanol and deionized water by sonication. Each pretreated GE was exposed to 2 μM H1 in hybridization buffer for 14 h at 4 °C, and the electrode was modified through Au–S affinity. The modified electrode was extensively rinsed with washing buffer to remove excess H1. Subsequently, the resultant electrode was blocked with 8 μL of MCH (1 mM) solution for 1 h to eliminate non-specific binding sites. For the telomerase extension reaction, 10 μL of telomerase extracts, 8 μL of telomerase primer (TP), and 2 mM of dNTPs in telomerase extension reaction buffer (TRAP buffer: 20 mM Tris-HCl pH 8.3, 1.5 mM $MgCl_2$, 0.005% Tween 20, 1 mM EGTA, 63 mM KCl, and BSA 0.1 mg mL^{-1}) were incubated at 37 °C for 60 min. Then, the solution was inactivated by heating it at 95 °C for 10 min to end the extension reaction. After that, the H1-modified electrode was immersed in telomerase extension product at 37 °C for 1 h. After washing with washing buffer, the resulting electrode was immersed in hybridization buffer containing Pt/MPC-COOH-H2 for 150 min at 37 °C, and then thoroughly rinsed with washing buffer. The biosensor performance was measured using differential pulse voltammetry (DPV) methods in 0.1 M PBS (pH 7.4).

3. Results and discussion

3.1. Characterization of the as-prepared samples

The morphologies of the as-prepared MPC-COOH and Pt/MPC-COOH were observed with SEM and TEM (Fig. 1). As shown in Fig. 1A and B, the SEM and TEM images of MPC-COOH exhibit a well-defined interconnected macroporous nanostructure, with an average pore size of 110 nm. The TEM image of Pt/MPC-COOH shows that Pt NPs were uniformly dispersed on the MPC surface (Fig. 1C). The EDX spectroscopy of the as-synthesized Pt/MPC-COOH shows the coexistence of C, Pt, W, and O (the strong peaks of Cu are from the copper grid), which further confirms the existence of Pt in the Pt/MPC-COOH nanohybrids (Fig. 1D).

XRD pattern of Pt/MPC-COOH is displayed in Fig. 2A. The characteristic peak at 25° corresponds to the plane of C (002). The characteristic peaks at 39.2°, 44.9°, 66.1°, and 78.9° correspond to the (111), (200), (220), and (311) planes of crystalline Pt, respectively [38]. Fig. 2B reveals that the negative zeta potential is greater for the as-prepared Pt/MPC-COOH-H2 compared to Pt/MPC-COOH, which confirms the successful conjugation of the DNA onto Pt/MPC-COOH. From the FT-IR spectrum of MPC-COOH (Fig. S1), the peaks at 1728 and 1596 cm^{-1} correspond to C═O stretching bands. Characteristic peaks were observed for the C–O stretching band from –COOH at 1375 cm^{-1}. Furthermore, the peak observed at 3400 cm^{-1} may be ascribed to O–H bands.

To prove that the formation of the Pt/MPC-COOH composites occurred, XPS was applied to analyze the chemical composition of the composite. As presented in Fig. S2A, the peaks at 35.9 eV, 72.1 eV, 274.4 eV, 283.5 eV, 426.2 eV, 530.2 eV can be respectively attributed to W 4f, Pt 4f, W 4d, C 1s, N 1s, and O 1s, demonstrating that the Pt/MPC-COOH composites were successfully synthesized. Furthermore, the W 4f spectrum exhibited two peaks at 35.9 and 38.1 eV, which could be ascribed to the W 4f5/2 and W 4f7/2 doublet, respectively (Fig. S2B). These binding energies suggest that W was in its full oxidation form in POMs when assembled in the composites [35,36]. The high-resolution spectrum of Pt 4f in Fig. S2C shows two binding energies of Pt 4f7/2 at 72.1 eV and Pt 4f5/2 at 75.4e V, which confirms that Pt nanoparticles were successfully doped onto the surface of MPC-COOH.

3.2. Feasibility of the proposed biosensor

Electrochemical impedance spectroscopy (EIS) is an efficient approach for probing the stepwise construction process of the sensor. The section of high-frequency semicircle diameter in the EIS results is related to the interfacial charge transfer resistance (R_{ct}). Fig. 3 shows that a small value of R_{ct} ($R_{ct} = 179\ \Omega$, curve a) was observed for the bare GE. After the immobilization of H1and the MCH, the value of R_{ct} significantly increased due to the electrostatic repulsion between negatively charged $K_3Fe(CN)_6/K_4Fe(CN)_6$ and the negatively charged DNA strands, and the blocking effect of MCH attenuated the electron transfer ($R_{ct} = 555\ \Omega$, curve b). When TP ($R_{ct} = 1.58\ k\Omega$, curve c) and Pt/MPC-COOH-H2 ($R_{ct} = 2.11\ k\Omega$, curve d) were successively incubated on the GE, a continuous increase of R_{ct} was observed, which occurred because the electron transfer was hindered. Therefore, the value of R_{ct} maintained a continuous enhancement from curves a to d, confirming the successful construction of this biosensor.

The feasibility of the proposed biosensing was further validated by polyacrylamide gel electrophoresis (PAGE), and the results are shown in Fig. S3. TP (lane a), H1 (lane c), and H2 (lane d) exhibited a distinct single migration band under the same conditions. When TP (lane a) was incubated with dNTPs and telomerase extracts at 37 °C for 1 h, a new band (lane b) would appear, demonstrating the formation of telomerase elongation products (TEPs). After the addition of H1 and H2, new bands (lane e) appeared, demonstrating that the TEPs can trigger hybridization between H1 and H2. This occurred because H2 replaces the TEPs to form the H1/H2 duplex through the CHA and simultaneous release of the

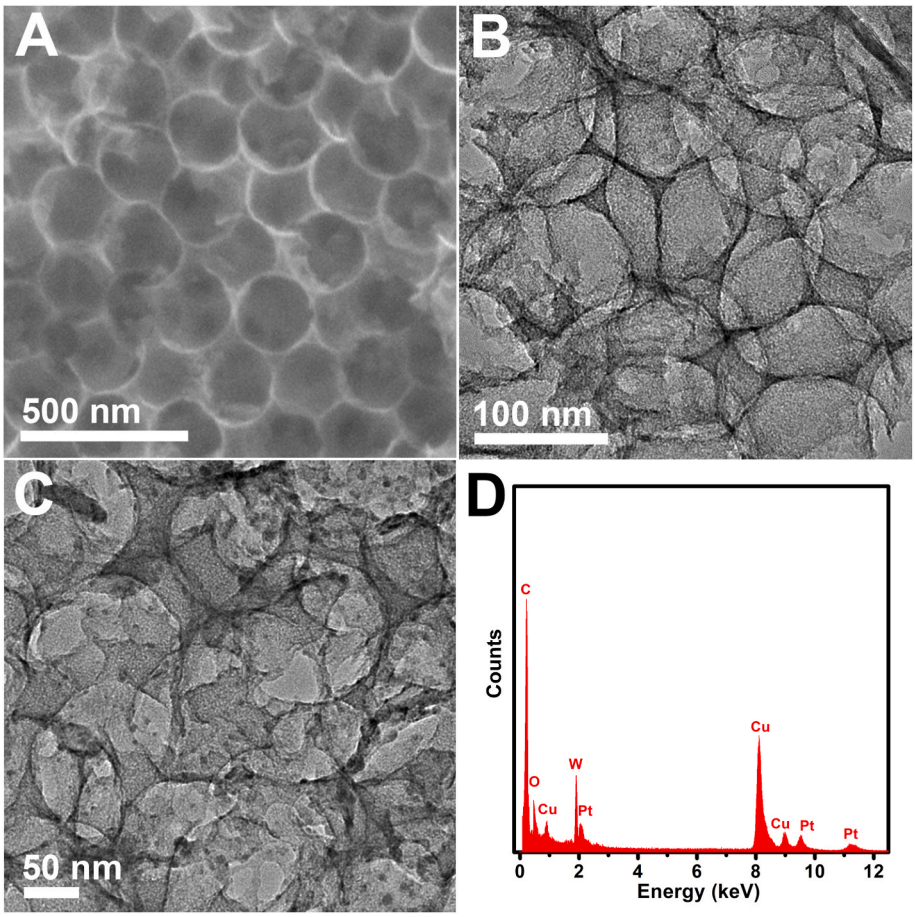

Fig. 1. SEM image of MPC-COOH (A). TEM images of MPC-COOH (B) and Pt/MPC-COOH (C). EDX spectrum of Pt/MPC-COOH (D).

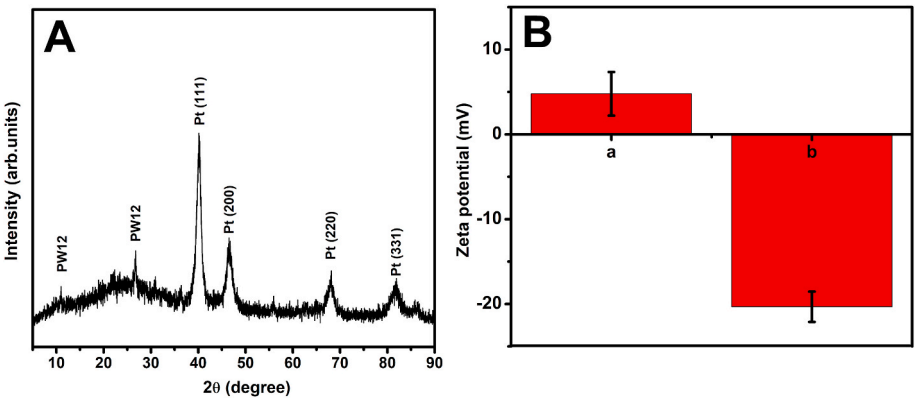

Fig. 2. XRD pattern of Pt/MPC-COOH(A). Zeta potentials of Pt/MPC-COOH (a) and Pt/MPC-COOH-H2 (b) (B).

TEPs. In the absence of telomerase extracts, no additional bands appeared (lane f), suggesting that no hybridization occurred between H1 and H2. The above results successfully indicate the interactions among these DNA sequences.

The DPV responses of different signal probes were also obtained to confirm the feasibility of the proposed biosensor (Fig. 4A). The bare GE (curve a) exhibited an obvious oxidation peak, which was attributed to the enhanced electron transfer process on the surface of electrode. After the immobilization of H1 and the blocking of the nonspecific adsorption sites by MCH, the DPV response barely appeared (curve b). After addition of the telomerase extracts and Pt/MPC-COOH-H2, the biosensor exhibited an obvious DPV response (curve c). This can be attributed to H1 hybridizing with Pt/MPC-COOH-H2, causing a mass of Pt/MPC-COOH-H2 that was introduced on the electrode surface and distinctly improved the DPV response. Additionally, a weak DPV response was obtained in the absence of telomerase extracts (curve d). After adding heat-treated cell extracts (curve e), a small increase in DPV response was observed as a result of the non-specific adsorption between Pt/MPC-COOH-H2 and the electrode surface.

3.3. *Optimization of the electrochemical biosensor*

The concentrations of H1, TP, and H2, the incubation time for telomerase-triggered elongation, and the CHA reaction time greatly

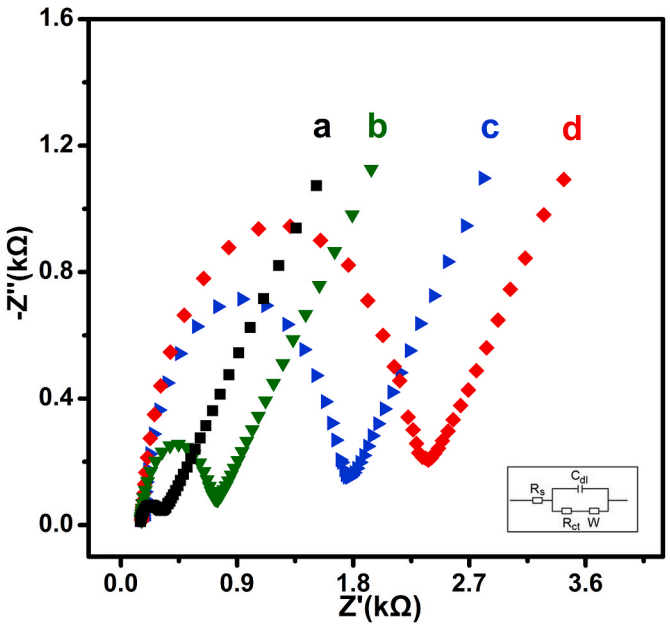

Fig. 3. EIS characterization of bare GE (a), MCH/H1/GE (b), cell extract + TP/MCH/H1/GE (c), and Pt/MPC-COOH-H2/(cell extract + TP)/MCH/H1/GE (d).

affect the electrochemical signal response. Therefore, five key experimental parameters were researched to obtain the optimal analytical experimental conditions. Fig. 4B reveals the effect of H1 concentration on the biosensor. When the H1 concentration was increased from 0.5 to 2 μM, the DPV intensity was gradually enhanced and reached a constant value at 2 μM. This suggested that the optimal concentration of H1 was 2 μM, and therefore, this value was applied to the following experiments. Fig. 4C shows the relationship between the concentration of TP and DPV intensity. With the increase in the TP concentration, the DPV intensity gradually increased until it was almost at the same value (2–4 μM). Therefore, in subsequent experiments, 2 μM was chosen as the optimal concentration for TP. As shown in Fig. 4D, the relationship between the incubation time for telomerase-triggered elongation and DPV intensity was investigated. With the increased incubation time for telomerase-triggered elongation, the DPV intensity increased accordingly and approached a plateau at 20 min. Hence, the optimal incubation time for telomerase-triggered elongation was determined to be 20 min. Fig. 4E shows that the DPV intensity was enhanced accordingly along with increasing H2 concentration from 0.5 to 2.5 μM. Then, the DPV intensity remained almost the same (2.5–10 μM). Hence, the optimum concentration of H2 was 2.5 μM. As shown in Fig. 4F, with the increase in the CHA reaction time, the DPV intensity gradually improved due to the combination of abundant Pt/MPC-COOH-H2 and the electrode. A plateau was reached after the CHA reaction time exceeded 150 min. Hence, we selected 150 min as the optimal CHA reaction time for subsequent experiments.

3.4. Telomerase activity assay

Under optimal conditions, a series of HeLa cells with different concentrations (from 10^2 to 10^7 HeLa cells mL^{-1}) was measured (Fig. 5). The DPV intensities were sequentially increased along with the increase in cell concentration. As shown in the inset plot of Fig. 5, the linear response range was from 10^2 to 10^7 HeLa cells mL^{-1} with a linear regression equation of $I_{(\mu A)} = 0.2913 \log(c) - 0.2043$, and the limit of detection (LOD) was calculated to be 9.02 HeLa cell mL^{-1} (S/N = 3). Moreover, the proposed biosensor has a wider dynamic range and lower LOD value than those of other published electrochemical telomerase biosensors (Table 1). Additionally, the biosensor exhibits outstanding reproducibility. The obtained relative standard deviation (RSD) of 2.84%, 2.49%, and 3.00% correspond to the five repetitive tests of 5.0×10^4, 3.7×10^5, and 1×10^6 HeLa cells mL^{-1}, respectively. The obtained signal intensities of the biosensor remained at 95.03% of its original response after storage at 4 °C for 15 days. This demonstrates that the proposed electrochemical sensing platform has satisfactory reproducibility and stability. In addition, the reproducibility was measured with different electrodes (n = 5). An acceptable RSD (3.57%) was obtained,

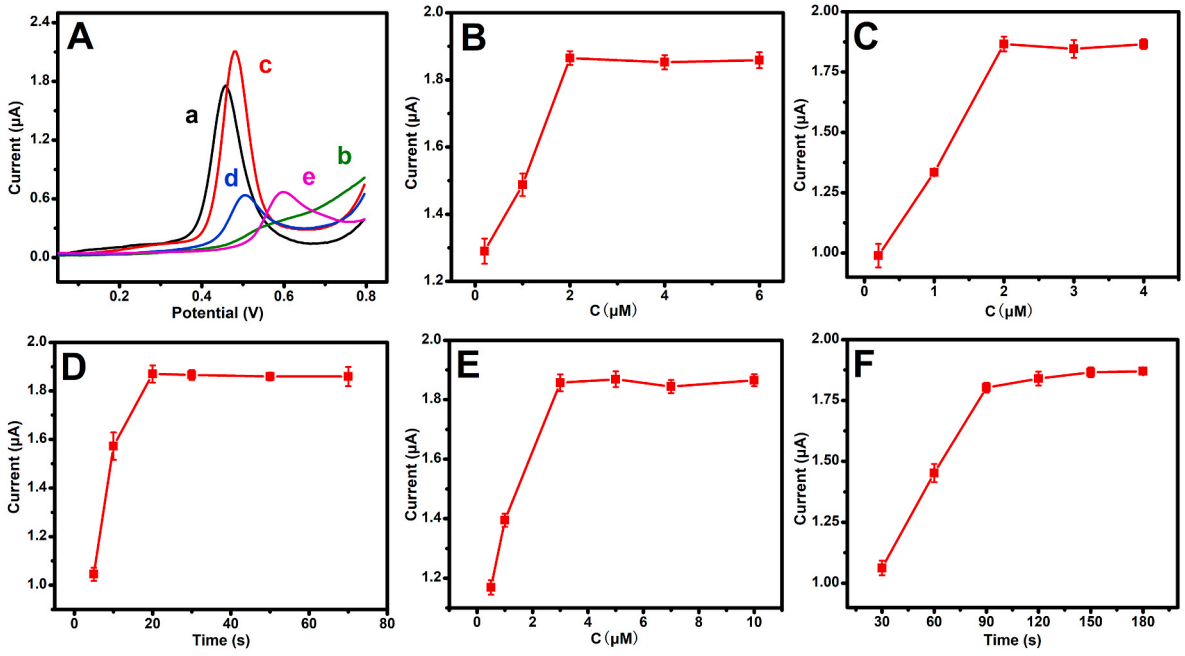

Fig. 4. DPV responses of bare GE (a), MCH/H1/GE (b), Pt/MPC-COOH-H2/(cell extracts + TP)/MCH/H1/GE (c), Pt/MPC-COOH-H2/TP/MCH/H1/GE (d), and Pt/MPC-COOH-H2/(heated cell extracts + TP)/MCH/H1/GE (e) in 0.1 M PBS (pH = 7.4) solution containing 0.3 mM of AP (A). Influence of the concentrations of H1 (B), the concentrations of TP (C), the incubation time for telomerase-triggered elongation (D), the concentrations of H2 (E) and the CHA reaction time (F) on DPV response currents. The HeLa cell number is equivalent to 3.7×10^5.

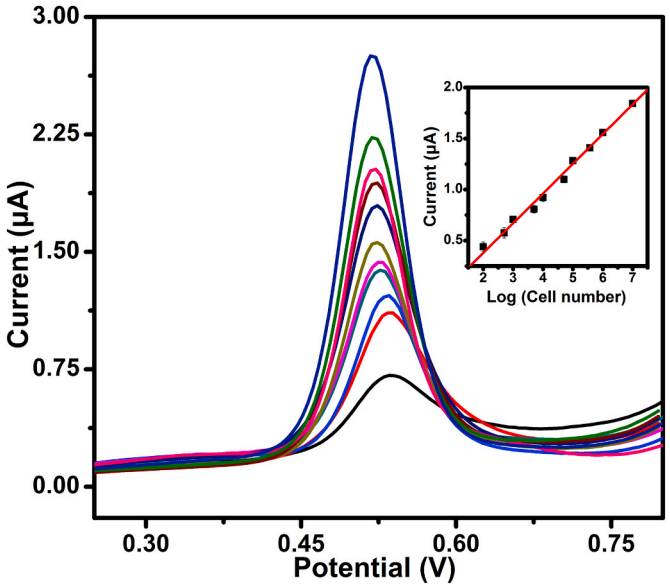

Fig. 5. DPV signals of the biosensor for telomerase extracts from different concentrations of HeLa cells at 1×10^2, 5×10^2, 1×10^3, 5×10^3, 1×10^4, 5×10^4, 1×10^5, 3.7×10^5, 1×10^6, and 1×10^7 (from bottom to up). Inset: calibration curve of DPV peak currents vs the logarithmic value of HeLa cell numbers.

which indicates that this method exhibits satisfactory reproducibility (Fig. S4). To further evaluate the analytical applicability of this method, recovery tests were further performed using 4 human blood serum samples (Table S2), and recoveries of 97.6–105.8% were obtained, which indicated that this method possesses excellent practicability in a complex biological system for telomerase activity assay.

In order to further estimate the universality of the developed telomerase activity detection, telomerase activity in different cancer cell lines, such as MDA-MB-23 and MCF-7, was measured. As revealed in Fig. 6, all of these cell lines exhibited remarkable DPV responses, revealing their excellent telomerase activities. A weak signal response was obtained for heated cell extracts because of the lack of telomerase activity. Furthermore, T4 DNA ligase (T4) and glucose oxidase (GOD) were selected as controls to explore the selectivity of the electrochemical sensing platform. In comparison with telomerase, GOD and T4 exhibited weak electrochemical signals (Fig. 6). These comparisons clearly confirm that the developed electrochemical sensing platform for telomerase activity assay possesses excellent universality and selectivity. The evaluation of inhibitory telomerase activity is displayed in Fig. S5.

4. Conclusions

In summary, we successfully developed a reliable and highly sensitive electrochemical biosensor based on the integration of the telomerase-initiated CHA process with electrocatalysis by Pt/MPC-COOH. The conjugation of Pt NPs with epoxy-functionalized MPC not only prevented the aggregation of Pt NPs, but also harnessed the excellent electrocatalytic performance of Pt NPs and the short electron-transport distance of epoxy-functionalized MPC, revealing outstanding catalytic activity toward AP oxidation. After the introduction of telomerase, TP could be extended to TEPs with several hexamer repeats (TTAGGG)n, which initiated the CHA cycle and lead to signal amplification. There was enrichment of Pt/MPC-COOH on the electrode surface, resulting in the increased electrochemical signal of the readout. This biosensor exhibits high catalytic performance such as low limit of detection (9.02 HeLa cells mL^{-1}) and wide linear response range (10^2 to 10^7 HeLa cells mL^{-1}) for telomerase activity detection. The electrochemical sensing platform exhibited an excellent analytical performance and good feasibility with cell extracts. This shows that the developed sensor can be a favorable analytical tool for the evaluation of telomerase activity in biological analysis.

Table 1
Comparison of different analytical strategies for telomerase activity detection.

Materials	Linear range (HeLa cells mL^{-1})	Limit of detection (HeLa cells mL^{-1})	Detection mode	Ref.
CS/Ru−PEI@ZIF-8/PtNPs[a]	50–1.0×10^6	11	EC[b]	[15]
T7 Exonuclease-Aided Target Recycling Amplification	2–1.0×10^3	1	DPV[c]	[18]
SNAs AuNPs[d]	10–1.0×10^4	2	DPV	[19]
PorMOF@SA[e]	100–1.0×10^7	30	DPV	[20]
ExoIII-aided target recycle amplification	5–1.0×10^3	1	DPV	[21]
STTS/GE[f]	0–5.0×10^4	10	i-t[g]	[22]
AuNRs-3-cDNA[h]	100–1.04×10^7	52.81	DPV	[23]
Pt@UiO-66-NH_2-cDNA[i]	500–1.0×10^7	100	LSV[j]	[24]
Gold nanoparticles	5–1.0×10^3	3	UV–Vis[k]	[39]
AuNP-DNA[l]	200–1.2×10^4	46	Fluorescence	[40]
Au@CeMOF-cDNA[m]	200–2.0×10^6	27	SWV[n]	[41]
H-GNs[o]	100–2.3×10^3	60	Colorimetry	[42]
Au NRs/TMB^{2+}[p]	200–1.5×10^4	90	Colorimetry	[43]
Au NPs-pDNA[q]	100–800 2.0×10^3–1.6×10^4	30	PEC[r]	[44]
Pd/MIL101-NH2-cDNA[s]	5.0×10^2–1.62×10^7	11.25	DPV	[45]
Pt/MPC-COOH-H2	100–1.0×10^7	9.02	DPV	This work

[a] Ruthenium polyethyleneimine complex doped zeolitic imidazolate framework-8, Pt nanoparticles, and chitosan solution modified on glassy carbon electrode.
[b] Electrochemiluminescence.
[c] Differential pulse voltammetry.
[d] Spherical nucleic acids gold nanoparticles.
[e] Streptavidin functionalized porphyritic metal-organic framework.
[f] Spired DNA tetrahedron TS primer modified gold electrode.
[g] Amperometric i-t curve.
[h] Capture DNA was conjugated with carboxylic group functionalized Au nanorods.
[i] Pt nanoparticles encapsulated metal-organic frameworks with capture DNA.
[j] Linear sweep voltammetry.
[k] Ultraviolet–visible spectroscopy.
[l] DNAzyme strands functionalized gold nanoparticle.
[m] Capture DNA was conjugated with cerium-based metal-organic frameworks functionalized with gold nanoparticles.
[n] Square wave voltammetry.
[o] Hemin-graphene nanomaterial.
[p] Au nanorods were gradually etched by oxidation state of 3,3′,5,5′ tetramethylbenzidine sulfate.
[q] Gold nanoparticles-labeled DNA probe.
[r] Photoelectrochemical.
[s] Pd nanoparticles anchored on amine functionalized Cr-based metal-organic frameworks with capture DNA.

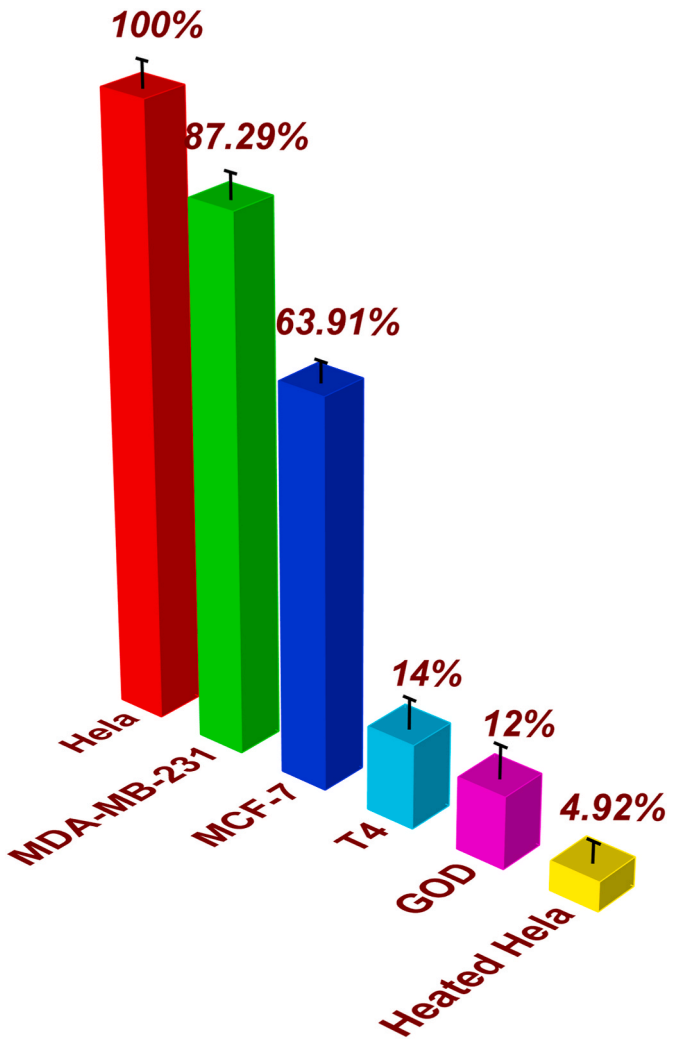

Fig. 6. Universality and selectivity of this electrochemical biosensor for the detection of telomerase activity.

Declaration of competing interest

The authors declare that they have no known competing financial interests or personal relationships that could have appeared to influence the work reported in this paper.

Acknowledgements

The authors gratefully acknowledge the support from the Priority Strategy Project of Key Laboratory of Medicinal Chemistry and Molecular Diagnosis of Ministry of Education (No. ts2019003), the Natural Science Foundation of Hebei Province (No. B2019201407 and No. B2018201214), the Science and Technology Project of Hebei Education Department (No. QN2020153), and the Advanced Talents Incubation Program of the Hebei University (No. 801260201026).

Appendix A. Supplementary data

Supplementary data to this article can be found online at https://doi.org/10.1016/j.talanta.2020.121957.

References

[1] J. Huang, L. Zhu, H. Ju, J. Lei, Telomerase triggered DNA walker with a superhairpin structure for human telomerase activity sensing, Anal. Chem. 91 (2019) 6981–6985.
[2] X. Li, Y. Cui, Y. Du, A. Tang, D. Kong, Label-free telomerase detection in single cell using a five-base telomerase product-triggered exponential rolling circle amplification strategy, ACS Sens. 4 (2019) 1090–1096.
[3] X. Yang, Y. Tang, S.D. Mason, J. Chen, F. Li, Enzyme-powered three-dimensional DNA nanomachine for DNA walking, payload release, and biosensing, ACS Nano 10 (2016) 2324–2330.
[4] L. Wang, T. Meng, D. Zhao, H. Jia, S. An, X. Yang, et al., An enzyme-free electrochemical biosensor based on well monodisperse Au nanorods for ultra-sensitive detection of telomerase activity, Biosens. Bioelectron. 148 (2020) 111834.
[5] H. Wang, H. Wang, C. Liu, X. Duan, Z. Li, Ultrasensitive detection of telomerase activity in a single cell using stem-loop primer-mediated exponential amplification (SPEA) with near zero nonspecific signal, Chem. Sci. 7 (2016) 4945–4950.
[6] Y. Chu, A.P. Deng, W. Wang, J.J. Zhu, Concatenated Catalytic hairpin assembly/hyperbranched hybridization chain reaction based enzyme-Free signal amplification for the sensitive photoelectrochemical detection of human telomerase RNA, Anal. Chem. 91 (2019) 3619–3627.
[7] Z. Dai, J. Guo, J. Xu, C. Liu, Z. Gao, Y.Y. Song, Target-driven nanozyme growth in TiO_2 nanochannels for improving selectivity in electrochemical biosensing, Anal. Chem. 92 (2020) 10033–10041.
[8] D. Zhu, W. Liu, D. Zhao, Q. Hao, J. Li, J. Huang, et al., Label-free electrochemical sensing platform for MicroRNA-21 detection using thionine and gold nanoparticles Co-functionalized MoS_2 nanosheet, ACS Appl. Mater. Interfaces 9 (2017) 35597–35603.
[9] S. Jiang, Y. Zhang, Y. Yang, Y. Huang, G. Ma, Y. Luo, et al., Glucose oxidase-instructed fluorescence amplification strategy for intracellular glucose detection, ACS Appl. Mater. Interfaces 11 (2019) 10554–10558.
[10] F. Su, L. Wang, Y. Sun, C. Liu, X. Duan, Z. Li, Highly sensitive detection of CpG methylation in genomic DNA by AuNP-based colorimetric assay with ligase chain reaction, Chem. Commun. 51 (2015) 3371–3374.
[11] H. Fan, H. Bai, Q. Liu, H. Xing, X.B. Zhang, W. Tan, Monitoring telomerase activity in living cells with high sensitivity using cascade amplification reaction-based Nanoprobe, Anal. Chem. 91 (2019) 13143–13151.
[12] X. Guo, X. Wu, M. Sun, L. Xu, H. Kuang, C. Xu, Tetrahedron probes for ultrasensitive in situ detection of telomerase and surface glycoprotein activity in living cells, Anal. Chem. 92 (2020) 2310–2315.
[13] T. Meng, D. Zhao, H. Ye, Y. Feng, H. Wang, Y. Zhang, Construction of an ultrasensitive electrochemical sensing platform for microRNA-21 based on interface impedance spectroscopy, J. Colloid Interface Sci. 578 (2020) 164–170.
[14] L. Meng, M. Liu, K. Xiao, X. Zhang, C. Du, J. Chen, Sensitive photoelectrochemical assay of Pb^{2+} based on DNAzyme-induced disassembly of the "Z-scheme" TiO_2/Au/CdS QDs system, Chem. Commun. 56 (2020) 8261–8264.
[15] C. Xiong, W. Liang, Y. Zheng, Y. Zhuo, Y. Chai, R. Yuan, Ultrasensitive assay for telomerase activity via self-enhanced electrochemiluminescent ruthenium complex doped metal-organic frameworks with high emission efficiency, Anal. Chem. 89 (2017) 3222–3227.
[16] R. Qian, L. Ding, L. Yan, M. Lin, H. Ju, Smart vesicle kit for in situ monitoring of intracellular telomerase activity using a telomerase-responsive probe, Anal. Chem. 86 (2014) 8642–8648.
[17] Y. Wang, L. Shi, J. Zhu, B. Li, Y. Jin, Visual and sensitive detection of telomerase activity via hydrogen peroxide test strip, Biosens. Bioelectron. 156 (2020) 112132.
[18] X. Liu, W. Li, T. Hou, S. Dong, G. Yu, F. Li, Homogeneous electrochemical strategy for human telomerase activity assay at single-cell level based on T7 exonuclease-aided target recycling amplification, Anal. Chem. 87 (2015) 4030–4036.
[19] W. Wang, J. Li, K. Rui, P. Gai, J. Zhang, J. Zhu, Sensitive electrochemical detection of telomerase activity using spherical nucleic acids gold nanoparticles triggered mimic-hybridization chain reaction enzyme-free dual signal amplification, Anal. Chem. 87 (2015) 3019–3026.
[20] P. Ling, J. Lei, H. Ju, Nanoscaled porphyrinic metal–organic frameworks for electrochemical detection of telomerase activity via telomerase triggered conformation switch, Anal. Chem. 88 (2016) 10680–10686.
[21] J. Li, J. Ma, Y. Zhang, Z. Zhang, K. Hu, Highly sensitive electrochemical analysis of telomerase activity based on magnetic bead separation and exonuclease III-aided target recycling amplification, Bioelectrochemistry 130 (2019) 107341.
[22] Y. Li, Y. Wen, L. Wang, W. Liang, L. Xu, S. Ren, et al., Analysis of telomerase activity based on a spired DNA tetrahedron TS primer, Biosens. Bioelectron. 67 (2015) 364–369.
[23] L. Wang, T. Meng, G. Yu, S. Wu, J. Sun, H. Jia, et al., A label-free electrochemical biosensor for ultra-sensitively detecting telomerase activity based on the enhanced catalytic currents of acetaminophen catalyzed by Au nanorods, Biosens. Bioelectron. 124–125 (2019) 53–58.
[24] P. Ling, J. Lei, L. Jia, H. Ju, Platinum nanoparticles encapsulated metal-organic frameworks for the electrochemical detection of telomerase activity, Chem. Commun. 52 (2016) 1226–1229.
[25] T. Meng, H. Jia, H. Ye, T. Zeng, X. Yang, H. Wang, et al., Facile preparation of $CoMoO_4$ nanorods at macroporous carbon hybrid electrocatalyst for non-enzymatic glucose detection, J. Colloid Interface Sci. 560 (2020) 1–10.
[26] H. Jia, M. Zhang, T. Meng, S. An, H. Wang, X. Yang, et al., Facile synthesis of Fe, Co bimetal embedded nanoporous carbon polyhedron composites for an efficient oxygen evolution reaction, J. Colloid Interface Sci. 563 (2020) 189–196.

[27] Y. Fu, F. Ding, J. Chen, M. Liu, X. Zhang, C. Du, et al., Label-free and near-zero-background-noise photoelectrochemical assay of methyltransferase activity based on a Bi_2S_3/Ti_3C_2 Schottky junction, Chem. Commun. 56 (2020) 5799–5802.
[28] H. Jia, N. Shang, Y. Feng, H. Ye, J. Zhao, H. Wang, et al., Facile preparation of Ni nanoparticle embedded on mesoporous carbon nanorods for non-enzymatic glucose detection, J. Colloid Interface Sci. 583 (2021) 310–320.
[29] L. Wang, T. Meng, H. Jia, Y. Feng, T. Gong, H. Wang, et al., Electrochemical study of hydrazine oxidation by leaf-shaped copper oxide loaded on highly ordered mesoporous carbon composite, J. Colloid Interface Sci. 549 (2019) 98–104.
[30] T. Yan, L. Zhu, H. Ju, J. Lei, DNA-walker-induced allosteric switch for tandem signal amplification with palladium nanoparticles/metal-organic framework tags in electrochemical biosensing, Anal. Chem. 90 (2018) 14493–14499.
[31] T. Meng, L. Wang, H. Jia, T. Gong, Y. Feng, R. Li, et al., Facile synthesis of platinum-embedded zirconia/porous carbons tri-component nanohybrids from metal-organic framework and their application for ultra-sensitively detection of methyl parathion, J. Colloid Interface Sci. 536 (2019) 424–430.
[32] Q. Teng, Y. Chen, X. Sun, Y. Wang, F. Li, L. Wang, et al., Formation of Fe_2O_3 microboxes/macroporous carbon hybrids from Prussian blue template for electrochemical applications, J. Alloy, Comd 739 (2018) 425–430.
[33] F. Li, R. Li, Y. Feng, T. Gong, M. Zhang, L. Wang, et al., Facile synthesis of Au-embedded porous carbon from metal-organic frameworks and for sensitive detection of acetaminophen in pharmaceutical products, Mater. Sci. Eng. C 95 (2019) 78–85.
[34] T. Meng, L. Wang, H. Jia, T. Gong, Y. Feng, R. Li, et al., Facile synthesis of platinum-embedded zirconia/porous carbons tri-component nanohybrids from metal-organic framework and their application for ultra-sensitively detection of methyl parathion, J. Colloid Interface Sci. 536 (2019) 424–430.
[35] L. Wang, T. Meng, J. Sun, S. Wu, M. Zhang, H. Wang, et al., Development of Pd/Polyoxometalate/nitrogen-doping hollow carbon spheres tricomponent nanohybrids: a selective electrochemical sensor for acetaminophen, Anal. Chim. Acta 1047 (2019) 28–35.
[36] T. Zhang, M. Liu, Q. Zhang, Y. Wang, X. Kong, L. Wang, et al., Sensitive determination of chlorogenic acid in pharmaceutical products based on the decoration of 3D macroporous carbon with Au nanoparticles via polyoxometalates, Analyst 142 (2017) 2603–2609.
[37] W. Stöber, A. Fink, E. Bohn, Controlled growth of monodisperse silica spheres in the micron size range, Colloid Interface Sci. 26 (1968) 62–69.
[38] T. Meng, A. Nsabimana, T. Zeng, H. Jia, S. An, H. Wang, et al., Preparation of Pt anchored on cerium oxide and ordered mesoporous carbon tri-component composite for electrocatalytic oxidation of adrenaline, Mater. Sci. Eng. C 110 (2020) 110747.
[39] J. Wang, J. Zhang, T. Li, R. Shen, G. Li, L. Ling, Strand displacement amplification-coupled dynamic light scattering method to detect urinary telomerase for non-invasive detection of bladder cancer, Biosens. Bioelectron. 131 (2019) 143–148.
[40] C. Xu, F. Zhang, K. Wang, E. Xu, Y. Liu, W. Wei, et al., A three-dimensional DNAzyme motor for sensitive imaging of telomerase activity in living cells, Sensor. Actuator. B Chem. 298 (2019) 126930.
[41] P. Dong, L. Zhu, J. Huang, J. Ren, J. Lei, Electrocatalysis of cerium metal-organic frameworks for ratiometric electrochemical detection of telomerase activity, Biosens. Bioelectron. 138 (2019) 111313.
[42] X. Xu, M. Wei, Y. Liu, X. Liu, W. Wei, Y. Zhang, et al., A simple, fast, label-free colorimetric method for detection of telomerase activity in urine by using hemin-graphene conjugates, Biosens. Bioelectron. 87 (2017) 600–606.
[43] D. Wang, R. Guo, Y. Wei, Y. Zhang, X. Zhao, Z. Xu, Sensitive multicolor visual detection of telomerase activity based on catalytic hairpin assembly and etching of Au nanorods, Biosens. Bioelectron. 122 (2018) 247–253.
[44] L. Zhang, X.-M. Shi, Y.-T. Xu, G.-C. Fan, Y.-Y. Liang, C. Wang, et al., Gold nanoparticle-Induced photocurrent quenching and recovery of polymer dots: toward signal-on energy-transfer-based photocathodic bioanalysis of telomerase activity in cell extracts, Anal. Chem. 91 (2019) 6403–6407.
[45] L. Wang, T. Meng, L. Liang, J. Sun, S. Wu, H. Wang, et al., Fabrication of amine-functionalized metal-organic frameworks with embedded palladium nanoparticles for highly sensitive electrochemical detection of telomerase activity, Sensor. Actuator. B Chem. 278 (2019) 133–139.